

Numerical Simulation of the Fragmentation Process of High Explosive Projectiles

Marinko Ugrčić¹⁾

The latest computational techniques, based on the finite element method (FEM), are developed to solve explicit dynamics problems and can be applied for the prediction of natural fragmentation of high explosive (HE) projectiles. The new methodology for numerical simulating performances of projectiles fragmentation integrates the FEM and the stochastic failure theory in the ANSYS AUTODYN[®] solver for two- and three-dimensional axis-symmetric analyses of the fragmentation process. This paper presents the results of the numerical analyses of the characteristics of fragmentation in terms of initial velocities, spray angle, fragment length and fragment mass distributions of a 105 mm HE projectile. The projectile fragmentation parameters depend on the projectile shape and size, casing thickness, explosive type, detonator size and position, etc. This paper focuses on the effects of the mechanical properties of the projectile casing material and the explosive type on the fragmentation characteristics. It was confirmed that the mechanical properties of the casing material have low effects on the initial velocities of fragments. Moreover, it was shown that a brittle casing material with low failure strain tends to produce a higher number of fragments with less average fragment mass. The comparison with some experimental data confirmed that the computed parameters of fragmentation predict properly the characteristics of casing disruption.

Key words: high explosive projectile, projectile fragmentation, 105mm caliber, numerical simulation, finite element method.

Introduction

AN explosion of high explosive projectile is always followed by shock loading, blast and fragmentation effects and response problems involve highly non-linear phenomena of a transient nature. So, a great range of physical processes must be taken into account in order to accurately characterize such events. There are three basic theoretical approaches that can be applied, together with more general skills such as experience and judgments, and these are outlined below.

Firstly, hand calculations (empirical formulas) can be applied. However, only the simplest highly idealized problems are practically solvable. More complex analytical techniques, which are usually computer-based or involve the use of look-up graphs and charts, are very useful in enabling consideration of many different cases, relatively quickly. But the analytical techniques are only applicable to a relatively narrow range of problems. This is because they are based on a limited set of experimental data or particular gross simplifying assumptions. Because of the difficulties in modeling the above-mentioned highly non-linear phenomena, physical experiments play an important role in the characterization of such problems. However, these experiments can be very costly and often difficult for instrumentation, acquisition and interpretation of results.

Numerical software based on the FEM offers another approach to blast, fragmentation and impact studies. Their advantage is that they model the full physics of the phenomena. In other words, they are designed to solve the governing conservation equations that describe the behavior of the considered physical system.

By their nature, numerical techniques are suitable for solving a wider range of problems than any particular analytical technique. They enable great savings to be made in the costs of research tests and they allow very different results analyses of a perfectly instrumented numerical experiment. Thus the parameters such as stress and strain of material, temperature, etc. that are virtually impossible to measure in the physical experiments can be examined in whatever appropriate detail.

In reality, numerical techniques for these highly non-linear phenomena are not able to model the complete physics without required data which must be obtained through experimental validation.

Despite the computational requirements of numerical analysis, the increased power and availability of computers has led to the widespread use of numerical software tools for solving highly non-linear dynamic problems. The barriers between experimentalists, analysts and designers are gradually breaking down as such tools become more widely used. Indeed, problems are most efficiently and effectively solved when a combined approach involving real testing, analytical methods and numerical techniques is taken.

A more general problem faced by all techniques, but which becomes particularly apparent when developing numerical techniques, is that many areas of non-linear response are insufficiently understood or poorly interpreted. A notable example is the details of dynamic material fracture that follows natural fragmentation of HE projectiles. Besides, the computation techniques based on the finite elements enable us to better visualize and understand these complex phenomena.

¹⁾ Mathematical Institute SASA, Kneza Mihaila 36, 11000 Belgrade, SERBIA

Regarding the analytical techniques of fragmentation analysis, there are the statistical and the physically based approaches [1]. The statistical modeling is based on the analysis of experimental data used in the definition of the mathematical description of the distribution of size, mass and shape of fragments. In a large number of papers [2-8] the authors deal with different statistical models of the fragments distribution. On the other hand, the authors have considered the physical approach to the fragmentation process based on the classical study of Mott [6]. The well-known Mott's initial fragmentation model was the basis for further, more complex research approaches to the modeling of fragmentation [2,6,7].

The calculation of fragmentation characteristics presented in the above-mentioned works apply specifically to cylindrical items and to items that can be reasonably approximated as either hollow cylindrical bodies or a series of hollow cylindrical sections [4,6-8]. If the variation in the thickness-to-diameter ratio is slight, the fragmentation characteristics may be calculated using average values over the entire length of the casing. However, if the variations are large, the casing is treated as a series of equivalent cylinders representing the actual shape as closely as possible. This principle, adopted on 105 mm M1 HE projectile casing [9], is illustrated in Fig.1 [7].

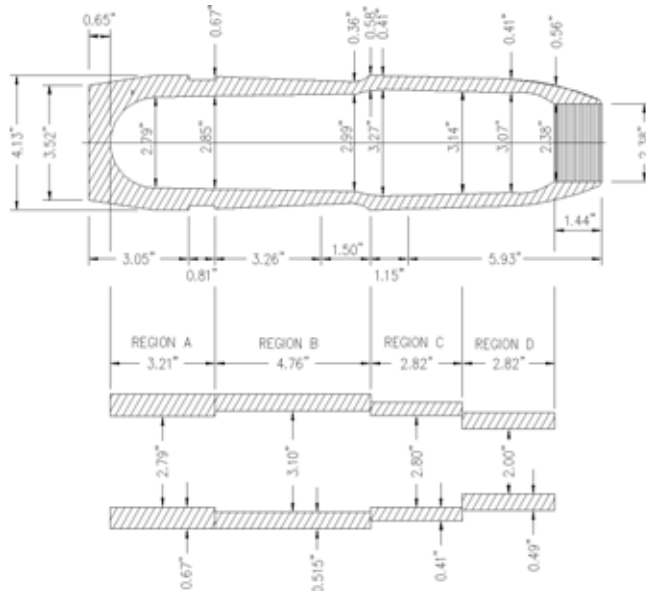


Figure 1. 105 mm M1 HE projectile - actual and final model geometries (original drawing from [7])

Generally, for this kind of fragmentation analysis, it is important to obtain the best description of the casing that is available. It can be achieved using the iteration procedure, providing the errors of the masses of the explosive charge and casing are less than 0.1 %. It should be noted that the base of the projectile is not a part of the hollow cylindrical shape and the fragmentation characteristics of the base may not be determined using the equations described in the above listed references. Similarly, the fuze well may not contain explosive material and, if this is the case, the fragments from this region may not be characterized by the methods described above.

In order to overcome the shown disadvantages of the given analytical approach (fragment analysis without considering the base of the casing and the fuze), the authors in [8] gave the detailed consideration of the casing fragmentation including the end sides of the projectile in the analysis.

For the purpose of this work, summarizing all the above considered advantages and disadvantages of the analytical and numerical techniques, the numerical method was chosen for the fragmentation analysis. The numerical software tools AUTODYN-2D® and AUTODYN-3D® [10], based on the finite element method, are used in the analyses of 105 mm HE projectile fragmentation (Fig.2).

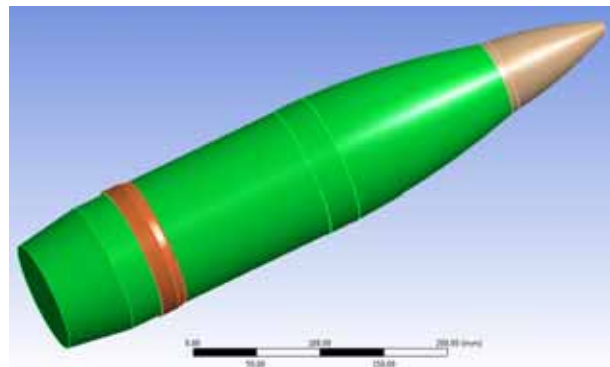


Figure 2. 3D model of a 105 mm HE projectile

The goal activities of the research presented in this work can be summarized as follows:

- numerical simulation of the fragmentation process varying the mechanical characteristics of the casing material and the type of filled explosive,
- determining the parameters of fragmentation: velocity, length and mass of fragments and fragments mass distribution based on the numerical experiments, and
- computing some practically immeasurable parameters such as temperature, stress and strain and strain rate in the considered materials.

Theoretical considerations

Model of the casing crack

When the high explosive charge detonates in a metallic cylinder (here projectile), several things occur. First, a detonation wave propagates along the axis of detonation (Fig.3). This results in the pressure being generated with the attendant stress being transferred to the metallic casing.

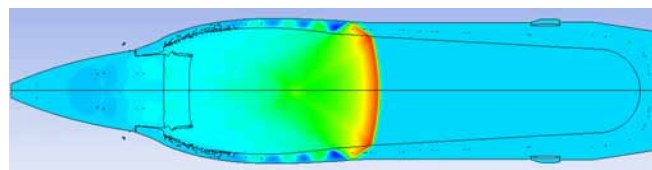


Figure 3. 2D model of the detonation wave propagation through explosive and the radial expansion of projectile casing ($t = 20 \mu s$)

The casing expands and, affected by a complex pressure field that generates the involved shock and expansion waves, after some time ruptures by shear or tearing failure. If the case expands significantly and removes significant energy from the detonation products, there is a condition known as a "terminal detonation". If the case expands very little before fragmenting, the result is known as a "prompt detonation". Once the case ruptures, fragments fly in directions dependent upon the initial rejection angle and velocity and their individual mass and geometry.

There are several factors that affect the fragmentation process: explosive brisance, charge to casing mass ratio, casing diameter, casing wall thickness and mechanical properties of the casing material, initiation, etc.

As already mentioned, the involved, very complex shock wave stresses¹ initiate the fragmentation of the casing. The fragmentation usually begins from the outside diameter through the formation of sharp radial cracks of longitudinal orientation. These cracks then join with shear cracks from the inside of the material (or not, if the material is extremely brittle). The cracks then coalesce into long, longitudinal cracks. If the casing material is resilient enough, as the casing expands radially and during this process, the wall will thin out somewhat. In any case, sooner or later, the metallic casing will fragment completely. The described scheme of casing fragmentation is depicted in Fig.4.

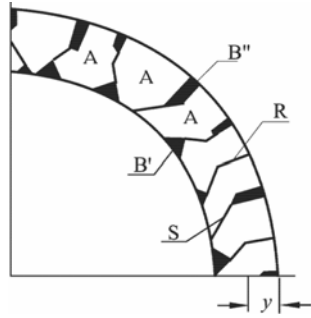


Figure 4. Scheme of casing rupture and fragments generating: (A) principal and (B) seed fragments

In the general case, regarding the morphology, two types of fragments arise [8]: large massive or principal fragments (A Type) and small light or seed fragments (B Type). The massive fragments comprise both casing surfaces from the inner and outer side and they are generated by principal stresses. On the other hand, the small fragments comprise one external surface (outer or inner) only.

The variety of small fragments includes two subtypes (Fig.5): B' - the fragments of the explosive contact zone formed by shear cracks and B'' - the fragments of the outer casing zone formed by the sharp rupture along the radial direction (typical for high-carbon steel).

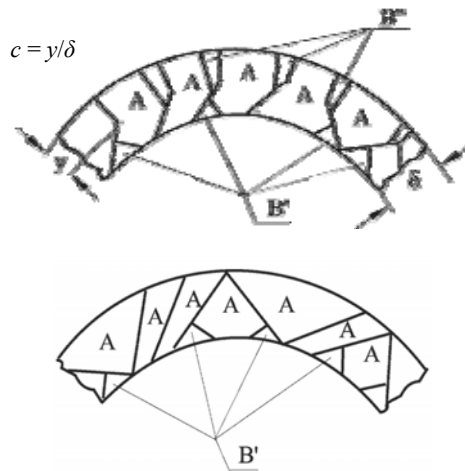


Figure 5. Casing crack scheme: brittle steel (up) and plastic steel (down)

The crack surfaces of principal massive fragments are characterized by two zones: the surfaces of brittle normal disruption (zone R in Fig.4) adjacent to the outer surface of the fragment and the surface of shear cracking along the sliding region (zone S in Fig.4) adjacent to the inner

fragment surface.

Denoting the zone of the brittle normal disruption y and wall thickness δ , then the type of cracking can be described by the ratio $c=y/\delta$. E.g. for the fragments of brittle materials such as gray cast iron, the typical values of c are between 0.5 and 0.8. For low-carbon steels and alloy steels, fragment generating occurs according to the scheme of shear crack and $c \approx 0$ (Fig.5, down). Besides the negative effect of high carbon contents, the mass of massive to small fragments ratio is directly proportional to the relative thickness of the casing and takes the values from 0.49 (thin-wall casing) to 0.91 (thick-wall casing) and more.

Furthermore, real fragmentation sand pit tests show that some metal mass of ruptured projectiles will be lost permanently for further analysis. In practice, the mass of so-called lost fragments may take a value up to 5% of the total mass of metal. It contains primarily very fine fragments (particles 0.5 to 500 mg of mass).

Some verified rules of casing fragmentation [12,13] based on material properties are confirmed here. In general, a more brittle material such as gray cast iron will produce a very large number of small fragments, and *vice versa*, a more resilient material will produce a smaller number of large fragments.

Stochastic Failure

To model the fragmentation for symmetric loading and geometry, it is necessary to impose some material heterogeneity. Real materials have inherent microscopic flaws which cause failures and cracking to initiate. An approach to reproducing this numerically is to randomize the failure stress or strain for the material. Using this property, a Mott distribution is used to define the variance in failure stress or strain. The Mott model assumes that elementary probability of an unfractured specimen of unit length will fracture when the strain increase from ε to $\varepsilon+d\varepsilon$ takes the exponential form:

$$C e^{\gamma \varepsilon} d\varepsilon \quad (1)$$

where ε is the strain, and C and γ are the parameters of material.

With the experimentally determined fracture stress σ_F and the strain ε_F , and the parameter in the strain-hardening law σ_P , the stochastic variance γ and parameter C will take an approximate form [3] as follows:

$$\gamma \approx 160 \frac{\sigma_P}{\sigma_F (1 + \varepsilon_F)} \quad (2)$$

$$C \approx \gamma e^{-(\varepsilon_F + 0.5772)} \quad (3)$$

So, the calculated values of C and γ based on equations (2) and (3) for different materials characteristics from Case #A to Case #D are given in Table 1.

Table 1. Mechanical and appropriate fracture parameters of material

	Fracture stress σ_F	Fracture strain ε_F	Strain-hardening σ_P	Stochastic variance γ	Parameter C
-	MPa	-	MPa	-	-
Case #A	800	0.63	450	55.2	2.42E-14
Case #B	800	0.25	510	81.6	6.33E-08
Case #C	700	0.25	450	82.3	5.38E-08
Case #D	900	0.25	450	64.0	4.04E-06

¹ An analysis of crack propagation using the strain energy density method in the case of classical mechanics problems (non shock wave loading) is explained in [11].

In accordance with the assumed model, each element of the casing is allocated a value of the fracture probability p , determined by the Mott distribution, where a value of one is relevant to the mechanical characteristics of the material.

The Mott probability distribution takes the form:

$$p = 1 - \exp\left\{-\frac{C}{\gamma}[\exp(\gamma\varepsilon) - 1]\right\} \quad (4)$$

where p is the probability of fracture.

For the implementation in explicit dynamics, the fracture strain of $\varepsilon=1$ is forced to be at a probability of 50%; therefore, the user needs only to specify the γ value and the constant C is automatically derived from this. The Mott probability distribution for more values of the stochastic variance γ , centered at the point ($p = 50\%$ and $\varepsilon = 1$), is shown in Fig.6.

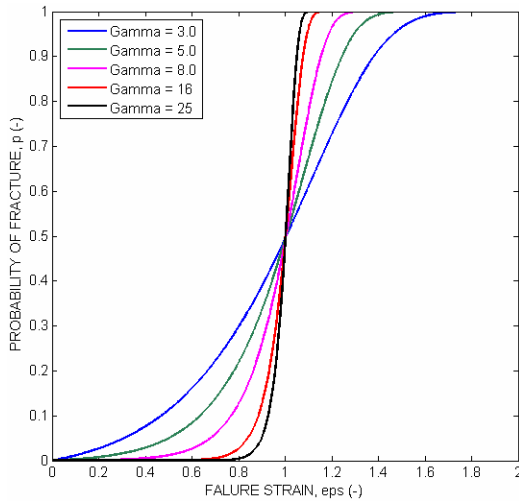


Figure 6. Mott distribution for varying the values of γ

The stochastic failure option may be used in conjunction with many of the failure properties, including hydrodynamic pressure (P_{\min}), plastic strain, principal stress and/or strain.

FEM modeling

Projectile modeling

Before the solution is initiated, the problems of equations of states, constitutive equations, specification of the geometry, initial and boundary conditions for all materials will be discussed.

A standard Jones-Wilkins-Lee (JWL) equation of state (EOS) was used to describe the adiabatic expansion of detonation products. The equation represents pressure as a function of the volume and energy:

$$p = A\left(1 - \frac{\omega\eta}{R_1}\right)e^{-\frac{R_1}{\eta}} + B\left(1 - \frac{\omega\eta}{R_2}\right)e^{-\frac{R_2}{\eta}} + e\omega\eta \quad (5)$$

where is: $\eta = \rho/\rho_e$ – ratio of density of detonation products and explosive charge and e – energy of detonation per volume unit. The values of constants A , R_1 , B , R_2 , and ω for very common explosives have been determined from dynamic experiments (cylinder test).

The dynamic responses of the steel casing, steel fuze parts, and the copper rotating band were modeled using a standard linear approximation or shock EOS [10] usually applied for metals. All necessary material coefficients in equations of state are given in solver library.

The elastic behavior of metallic materials is determined by Hook's Law relations between the deviator of stress rates and the strain rates. A pragmatic approach in the choice of yield criteria is a formulation given by the Von Mises yield criterion that describes the elastic limit and transition to the plastic flow. This applied criterion provides a relatively smooth and continuous yield surface. The state that, given the principal stresses σ_1 , σ_2 and σ_3 , the local yield condition is:

$$(\sigma_1 - \sigma_2)^2 + (\sigma_2 - \sigma_3)^2 + (\sigma_3 - \sigma_1)^2 = 2Y^2 \quad (6)$$

where is: Y – the yield strength in simple tension.

Used to model materials, typically metals, subjected to large strains, high strain rates and high temperatures, Johnson Cook strength equation defines the yield stress, Y , as a function of strain, strain rate and temperature:

$$Y = [A + B\varepsilon_p^n][1 + C \log \dot{\varepsilon}_p^*][1 - T_H^m] \quad (7)$$

where is: ε_p – effective plastic strain; $\dot{\varepsilon}_p^*$ – normalized effective plastic strain rate; A , B , C , m and n – constants of material determined experimentally and available in solver materials library, T_H – homologous temperature $T_H = (T - T_{\text{ref}})/(T_{\text{melt}} - T_{\text{ref}}) = (T - 300)/(T_{\text{melt}} - 300)$ K.

The expression in the first set of brackets gives the stress as a function of strain when $\dot{\varepsilon}_p^* = 1.0$ and $T_H = 0$ (i.e. for laboratory experiments at room temperature). The constant A is the basic yield stress at low strains while B and n represent the effect of strain hardening. The expressions in the second and third sets of brackets represent the effects of strain rate and temperature, respectively. In particular, the latter relationship models the thermal softening so that the yield stress drops to zero at the melting temperature T_{melt} .

The constants in these expressions were obtained by Johnson and Cook empirically by means of dynamic Hopkinson bar tensile tests over a range of temperatures. As well, the constants of the material were checked by calculations of Taylor tests of impacting metal cylinders on rigid metal targets which provided strain rates in excess of $10E+5 \text{ s}^{-1}$ and strains in excess of 2.0.

The plastic flow algorithm used with Johnson Cook model has an option to reduce high frequency oscillations that are sometimes observed in the yield surface under high strain rates. In this way, a first order rate correction is applied in the solver by default [10]. Also, a specific heat capacity of material must be defined to enable the calculation of temperature for thermal softening effects.

The air and explosive materials are modeled using the Euler solver where it is able to treat multi-material effects in one finite elements mesh. The Lagrangian meshing was used to describe the behavior of projectile metallic parts.

A 105 mm HE projectile was used to illustrate this modeling technique and the calculation of fragmentation characteristics. Fig. 7 depicts the initial coupled Lagrange-Euler meshing and the geometry of the 105 mm projectile given in the pre-processing procedure.



Figure 7. Initial 2D model of the 105 mm HE projectile generated in the coupled Euler-Lagrange mesh (axial half-section)

The generated Euler mesh is fine sizing with cells dimensions 1×1 mm.

After initial studying and partial testing, a convenient ways of pre-processing and numerical simulation were chosen. Firstly, the metallic parts design and meshing were achieved using two ANSYS solvers: design modeler and finite element modeler. Finally, after materials definition and assignment of the appropriate initial and boundary conditions, the designed models were converted into the solver AUTODYN®. 2D and quarter 3D axis-symmetry finite elements models were adopted for the simulation.

The numerical simulation of the 105 mm HE projectile fragmentation was carried out varying some features of materials of the projectile casing and the explosive charge. The assumed combinations of the used material for five specimens from Case #1 to Case #5 are shown in Table 2.

Table 2. Review of the used materials for projectile parts

	Casing	Explosive charge	Fuze	Rotating band
	Material	Type	Material	Material
Case #1	Steel #1	TNT	Steel #0	Copper
Case #2	Steel #2	TNT	Steel #0	Copper
Case #3	Steel #3 ($A_t=0.25$)	TNT	Steel #0	Copper
Case #4	Steel #3 ($A_t=0.10$)	TNT	Steel #0	Copper
Case #5	Steel #3	Comp. B	Steel #0	Copper

Regarding the analysis of the effects of material properties on the fragmentation process, various mechanical characteristics of the steel casing are considered. Table 3 contains the main mechanical properties of the casing material.

Table 3. Mechanical parameters of the casing material

	Density ρ	Tensile yield strength R_{eH}	Specific heat capacity c	Failure strain A_t
-	kg/m ³	MPa	J/kgK	-
Steel #0	4000	800	476.99	0.25
Steel #1	7890	600	451.99	0.25
Steel #2	7830	800	476.99	0.25
Steel #3	7750	1500	476.99	0.25/0.10

Let us say that a complex artillery fuze design was very simplified and modeled as a homogenous steel body with 4000 kg/m^3 of artificial density. This is suitable in this kind of analyses without the negative repercussions on the accuracy of the results.

The projectile was modeled based on the accepted physical properties of the materials and the design geometry. The computed physical and geometrical parameters of projectile parts together with the number of generated finite elements for full three-dimensional models of each item are given in Table 4.

Table 4. Physical and geometrical parameters of the projectile components

Part	Material	Volume V	Density ρ	Mass m	Number of FE
-	-	m ³	kg/m ³	kg	-
Casing	Steel	1.473E-03	7890	11.532	1824732
Rotating band	Copper	2.366E-05	8960	0.212	31488
Explosive charge	TNT	1.340E-03	1520	2.036	65352
Fuze body	Steel	2.058E-04	4000	0.823	25340
Fuze detonator	TNT	2.699E-05	1630	0.044	11356
Detonator	TNT	1.392E-04	1520	0.212	33212
Detonator body	Al alloy	2.331E-05	2750	0.064	1956
Sum	-	-	-	14.923	1993436

The data given in Table 4 were used to calculate the mass of metallic parts, explosive and fuze. Their computed mass and their appropriate real mass, shown in Table 5, coincide well.

Table 5. Review of the computed and real masses of the projectile parts

Part	Computed mass (Real mass)		
	Metallic parts	Explosive	Fuze
-	kg	kg	kg
Casing	11.532 (11.812)	-	-
Rotating band	0.212	-	-
Explosive charge	-	2.037	-
Fuze body	0.823	-	0.823
Fuze detonator	-	-	0.044
Detonator	-	0.212	-
Detonator body	0.064	-	0.064
Sum	12.631 (12.738)	2.249 (2.217)	0.931 (0.957)

Results and discussion

Expansion of the projectile casing during detonation

More sequences of the expansion of detonation products and the casing rejection computed for the coupled Euler-Lagrange model of the detonated projectile, from $t = 25 \mu\text{s}$ to $t = 75 \mu\text{s}$, are shown in Fig. 8.

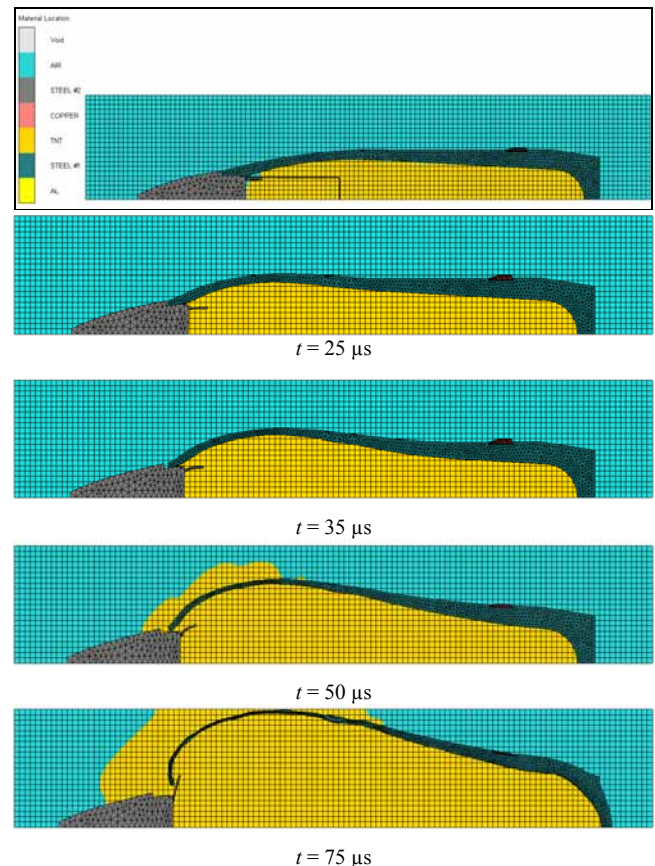


Figure 8. 2D expansion model of the projectile casing

The expansion of the casing occurs inside the Euler mesh filled by air considered as a perfect gas. During the expansion of the casing, loaded initially by the detonation wave and further pushed by the pressure of the gaseous products of detonation, its disruption appears. At this moment, the gaseous products of detonation began to leak through cracks (two last sequences in Fig. 8).

Physical parameters of the casing expansion during detonation

As previously mentioned, the actual computation technique represents a powerful instrument for successfully recording (computing) various physical parameters of an explosive process that are immeasurable in real experiments. Some kinds of such parameters of the expanded steel casing affected by the detonation of TNT (Case #5) at $t = 52.5 \mu\text{s}$ are illustrated and discussed below. At the given moment, the wall of the casing base is intensively stressed due to the involved shock wave.

Fig.9 illustrates the effective plastic strain in the wall of the 3D model of the projectile casing. The reached values of the plastic strain are extremely high, up to value of $\varepsilon_p = 1.152$.

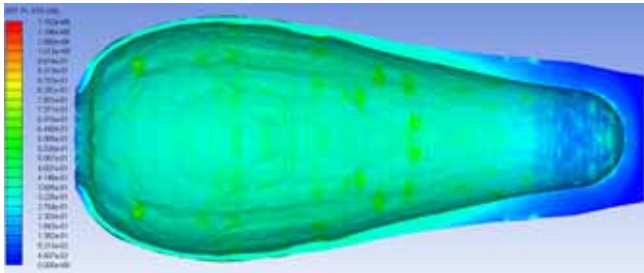


Figure 9. Plastic strain of the unruptured projectile casing ($t = 52.5 \mu\text{s}$)

The strain rate distribution of the projectile casing is given in Fig.10. The maximum computed value $\dot{\varepsilon}_p = 6.053\text{E}+5 \text{ s}^{-1}$ of the strain rate is reached on the casing base.

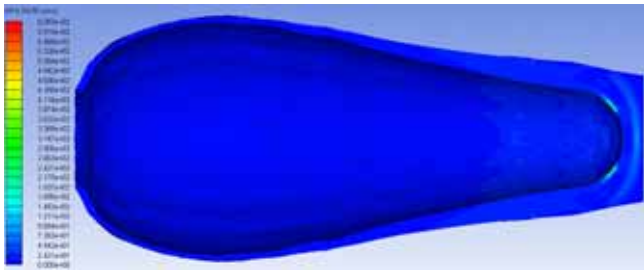


Figure 10. Strain rate of the unruptured projectile casing ($t = 52.5 \mu\text{s}$)

The temperature is distributed as in Fig.11. It is ranged from ambient temperature 300 K on the casing base to the maximum temperature of 849 K on the cylindrical part of the casing.

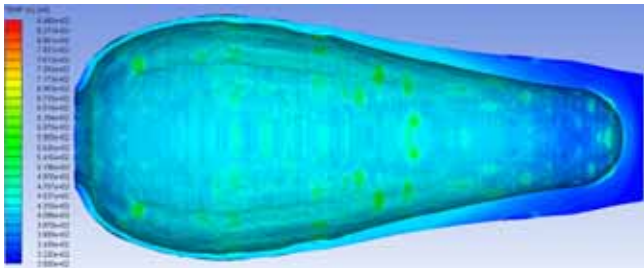


Figure 11. Temperature of the unruptured projectile casing ($t = 52.5 \mu\text{s}$)

Finally, Fig. 12 depicts the vector velocity distribution of fragments and unfragmented elements of the casing.

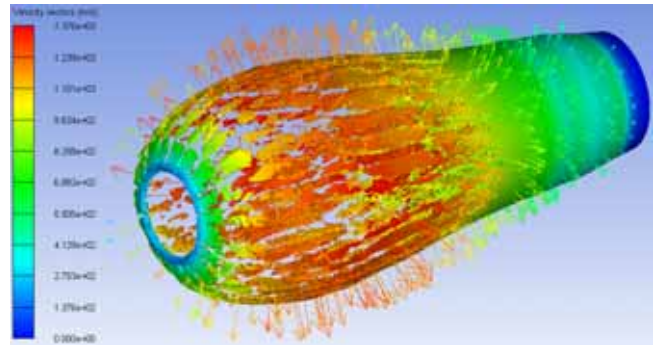


Figure 12. Fragments velocity of the ruptured projectile casing ($t = 52.5 \mu\text{s}$)

According to the last illustration, some fragments of the projectile casing intensively accelerate until the velocity of 1376 m/s.

In addition, the temperature and the velocity were registered in more gauge points located along the projectile (Fig.13).

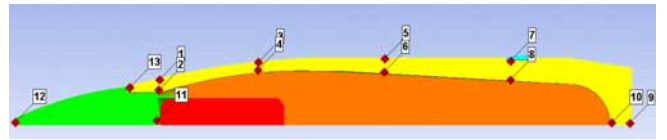


Figure 13. Gauge points allocation

The time history of acceleration and oscillatory velocity increasing in more opposite points on the inner and outer side of the casing wall is given in Fig.14.

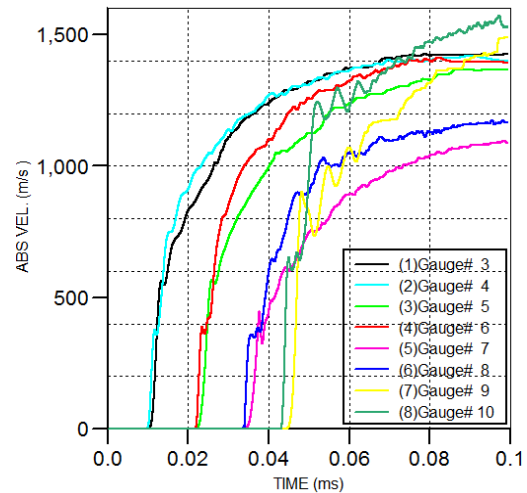


Figure 14. Time history of the velocity variation on the inner and outer side of the casing (Case #5)

The time history of the temperature variation on the inner and outer side of the casing is shown in Fig.15. The present discontinuities of the graph indicate the end of the formation of fragments containing considered gauges. At this moment, a rapid heating of fragments material stops because the intensive material deformation and inter-crystal friction fail. This is due to the inconsistency in the temperature range on the identical points located on the unruptured and on the fragmented casing (fragments). In any case, it can be expected that the temperature of fragments will be lower than the appropriate temperature of the unfractured casing.

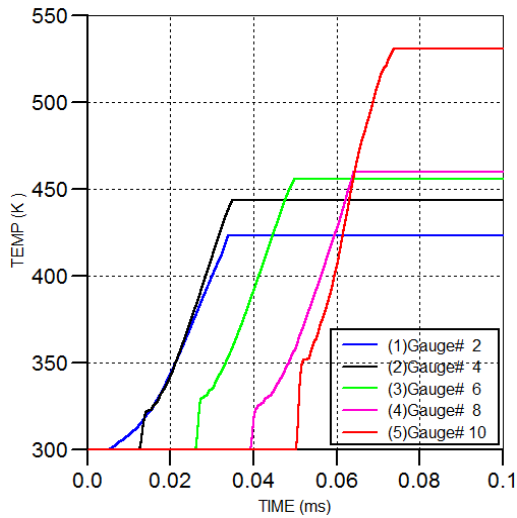


Figure 15. Time history of the temperature variation on the inner and outer side of the casing

Fragmentation of the projectile casing

The fragmentation progress of the 3D model of the projectile loaded by the shock wave and pressure of gaseous products of detonation is given in Fig.16.

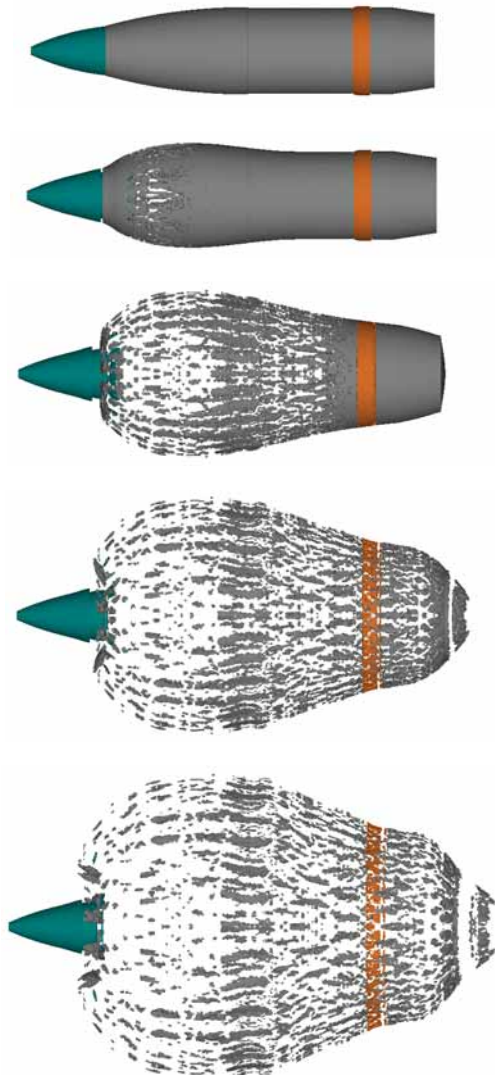


Figure 16. Fragmentation of the 105 mm HE projectile casing (Case #2): $t = 0, 30, 60, 90$ and $120 \mu s$

The nose and tail sections will break up into a small number of relatively massive fragments moving at velocities up to about 1.000 m/s. In particular, according to Fig.16, the geometry of the casing base with the hemispherical end of the inner side of the 105 mm HE projectile shows more favorable fragmentation behavior. On the other hand, the ogival and cylindrical parts will fracture into many smaller fragments travelling at different speed values up to 1500 m/s.

Status of the fuze and the rotating band

The numerical analysis is able to analyze the behavior of the fuze and the rotating band of the detonated projectile. A typical appearance of the fragmented fuze and the rotating band are given in Figures. 17 and 18, respectively.

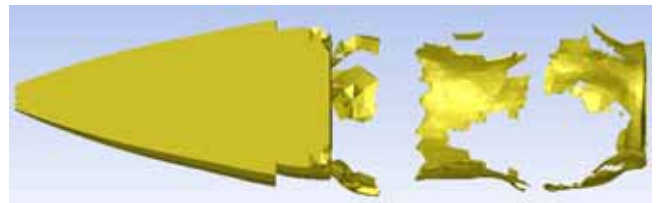


Figure 17. Fuze and detonator body disruption $50 \mu s$ after the detonation

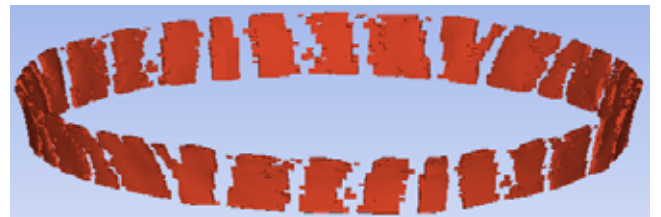


Figure 18. Rotating band disruption $100 \mu s$ after the detonation

The rejected fuze keeps usually consistency after the detonation. Fig.19 shows the time history of the velocity registered by two gauges (#11 and #12 in Fig.13) allocated on the front and the end side of the fuze body.

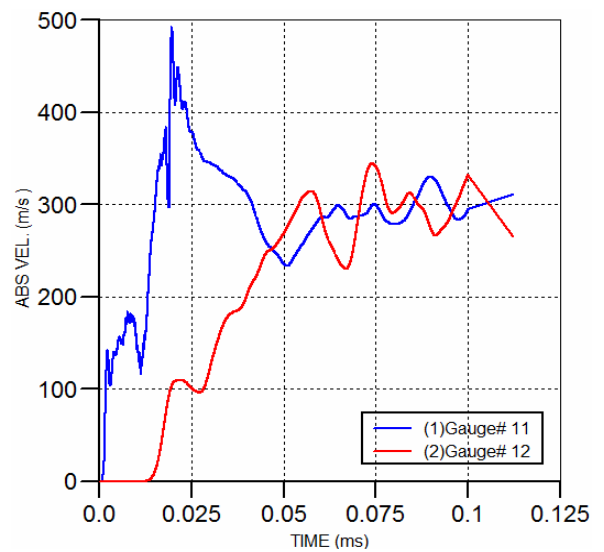


Figure 19. Time history of the velocity variation of the fuze

According to the diagram of velocities, after more oscillations the material of the fuze will take the final or so-called terminal velocity (~ 300 m/s).

Effect of the yield strength and failure strain of the casing material

The computed results (Case #1 to Case #5) that describe the fragmentation process are given in Table 6.

Table 6. Parameters of the fragmentation

	Total			Fragm. mass $1 \leq m \leq 50$ g		
	Number N	Average length L	Average kin. energy E_{kin}	Average mass M	Min. mass M_{min}	Max. mass M_{max}
-	-	mm	kJ	g	g	g
Case #1	1609	12.611	1.014	3.742	1.022	23.320
Case #2	1577	13.624	1.332	4.051	1.001	20.680
Case #3	1331	17.656	2.892	7.200	1.018	49.150
Case #4	1451	8.316	0.317	2.371	1.008	11.980
Case #5	1412	16.142	2.816	6.327	1.003	43.900

The average length of fragments L in Table 6 is calculated according to the relation:

$$L = \frac{\sum_{i=1}^{i=N} l_i}{N} \quad (8)$$

where is: l_i – the length of the current fragment and N – the total number of fragments.

The effects of the yield strength of the projectile casing on the characteristics of projectile fragmentation can be analyzed through the rupture results of Cases #1 to #3 (Table 6). The analysis of Case #1 with the lowest yield strength of the projectile casing gives the highest number of fragments and the lowest average kinetic energy per fragment whilst the casing with the highest yield strength (Case #3) gives the lowest number of fragments and the highest average kinetic energy per fragment. It must be noted that this average kinetic energy is the energy of the fragment after final cracking and accelerating when it starts to fly freely.

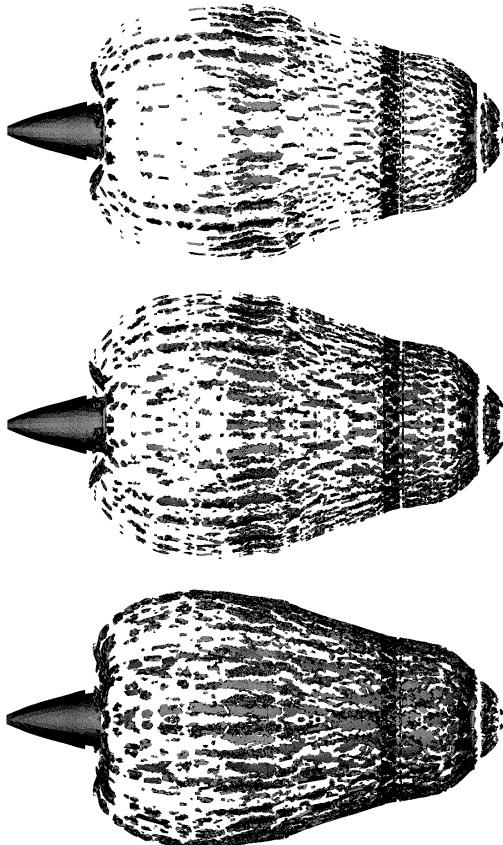


Figure 20. Effect of the casing material properties on projectile fragmentation: from top to bottom - Case #1, #2 and #3 ($t=95 \mu s$)

An appearance of disrupted projectile casings, given by computer simulation for Cases #1 to #3 (Fig.20), clarifies the effect of the casing yield strength on the fragmentation process and the number and size of fragments.

The effects of the failure strain of the casing material are considered through the analysis of fragmentation for Case #3 and Case #4. It can be seen that, all other conditions being the same, lower failure strain gives a higher number of fragments compared to those produced from the case material with higher failure strain. The average kinetic energy per fragment in Case #4 is not higher due to its high number of fragments and very early rupture initiation caused by the low value of failure strain.

Despite the good fragmentation, the average kinetic energy in Case #4 is the lowest. This fact indicates that the missile designers have to be very careful in the choice of the casing material.

Analysis of the distribution of the mass and length of fragments

The distributions of normalized fragment mass m/M depending on the normalized fragment number n/N are derived based on the simulated fragmentation of Cases #1 to #3 and shown graphically in Fig.21. The curves are given for the representative specimen of masses $1 \leq m \leq 50$ g.

In addition, a relationship between the normalized fragment length l/L and the normalized fragment number is depicted as a log-log diagram in Fig.22. Here are considered the lengths of all fragments without the fragments generated from the fuze.

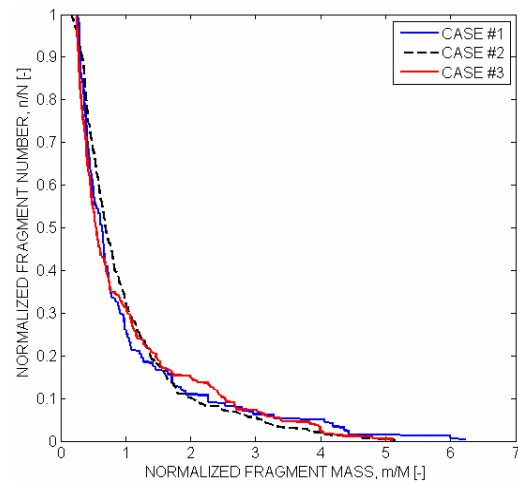


Figure 21. Normalized distribution of the mass of fragments

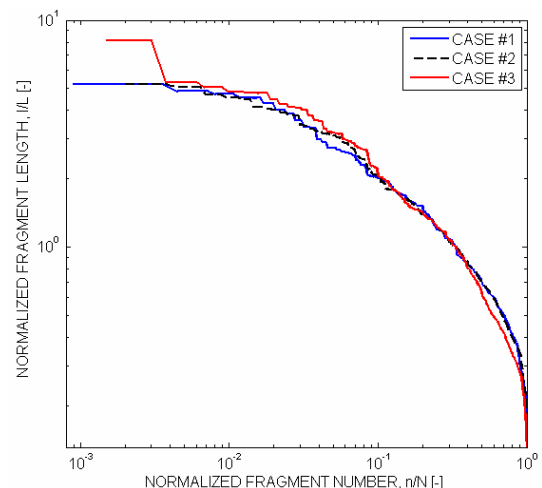


Figure 22. Normalized distribution of the length of fragments

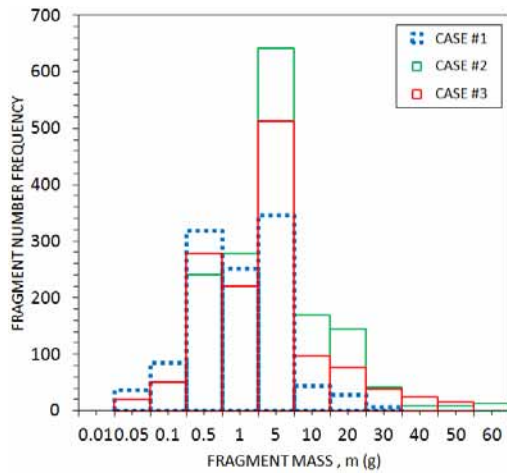


Figure 23. Fragment number frequency vs. fragment mass

According to the data in Table 6 and Figures 21 and 22, the casing material of the highest mechanical properties (Case #3), relatively close to high-alloy steels, will produce the lowest number of fragments, but fragments of the highest mass and appropriate the highest size.

Fig.23 depicts the fragment number frequency depending on the particular fragment mass for Cases #1 to #3. The considered masses are between 0.01 g and 65 g.

The histograms represent one of the forms of the so-called fragmentation law more frequently used to describe the fragmentation of HE projectiles. It indicates that the mass of fragments will be ranged most frequently from 3 g to 7.5 g. The calculated average values of fragment mass for all three cases, given in Table 6, coincide with the given interval as well.

Fragment spray angle

The numerical simulation of the distribution of the fragment rejection angle β along the casing length l_c is obtained for Cases #1 to #3, including the fragments formed out of the projectile casing and the rotating band. Fig.24 depicts this distribution in the meridian plane of the projectile casing where β varies from -90° to $+90^\circ$. The length of the projectile casing is $L_c = 399$ mm.

A slope angle of the velocity vector of the fragments is considered relative to the y -axis, orthogonal to the symmetry axis of the projectile casing. The angle β will be negative for fragments generated from the ogival part of the casing giving the front spray of the fragments. On the other hand, for the cylindrical part and the casing base, the angle β will be positive generating, here denoted, the rear spray of fragments.

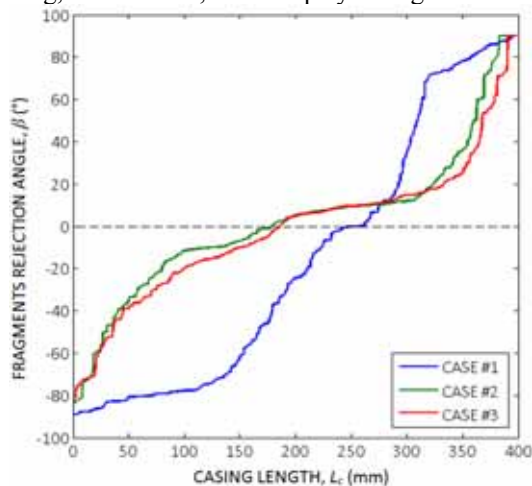


Figure 24. Distribution of the fragment rejection angle along the casing length

Regarding the mechanical properties, a preliminary analysis of the diagram in Fig.24 indicates that the casing material of the lower tensile yield strength (Case #1) might not provide the best fragments efficiency of the HE projectile but it provides the widest range of the spray angle of fragments covering the largest surrounding area.

Table 7 illustrates the main characteristics of the fragment spray for the above-mentioned cases.

Table 7. Parameters of the fragment spray angle

	Front spray angle $-\beta_{\max}$	Back spray angle $+\beta_{\max}$	Average spray angle β_{av}
	($^\circ$)	($^\circ$)	($^\circ$)
Case #1	-89.81	90	0.19
Case #2	-84.07	90	3.11
Case #3	-83.61	90	1.65

It can be seen that the mechanical properties of the material of the projectile casing affect chiefly the average spray angle of fragments β_{av} and their front spray angle $-\beta_{\max}$.

Effect of the explosive type

The effect of the type of filled explosive will be discussed based on the computed results for Case #3 and Case #5. When comparing the total number of fragments, the average mass and size of the fragments, and the average kinetic energy, the HE projectile filled with explosive of better detonating properties (Comp B in Case #5) will provide a higher number of fragments and somewhat lower other parameters.

Velocity of fragments

The summary analysis of the velocity distribution is given in Fig.25. The fragment of the highest mass, here the body of the fuze ($m_f = 712$ g), will take the lowest average velocity (313.4 m/s). The velocities of other parts are varying from 313.4 m/s to 1550 m/s. Maximum velocities belong to the fragments of the projectile casing made of the material of the highest mechanical characteristics (Case #3).

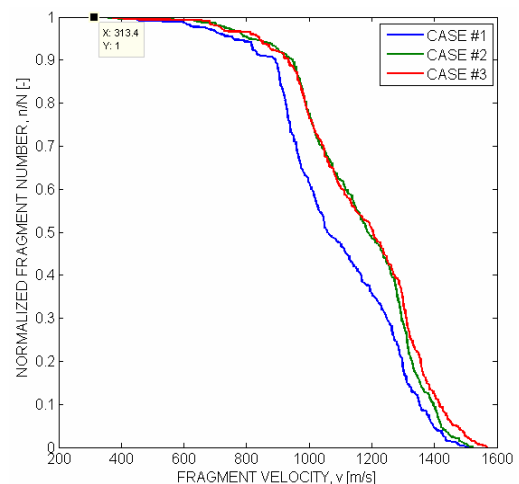


Figure 25. Normalized fragment number vs. fragment velocity

Additionally, some relations between the fragment mass and the fragment velocity will be illustrated. This kind of non-uniform distribution for Case #2 is given in Fig.26.

According to Fig.26, the proportional rule: the higher fragment mass – the higher fragment velocity, is not applicable here. It is because the distribution of the fragment velocity depends primordialy on the considered casing region and appropriate local conditions of the casing rejection.

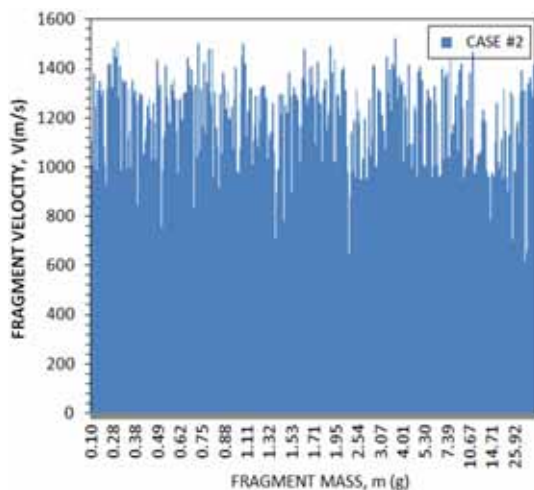


Figure 26. Distribution of the fragment velocity depending on the fragment mass

Finally, we have to emphasize that this paper was intentionally designed to demonstrate the possibilities of the method based fully on the FEM techniques and the solver ANSYS AUTODYN® in solving the explicit problem of projectile fragmentation. Therefore, more detailed statistical analyses of the computed data, e.g. defining the best analytical equation of the fragmentation law and other relevant statistical parameters for the estimation of the fragmentation process are missing here. In the same way, the comparative analysis of the computed results and the experimental data was greatly reduced.

One example only is considered to compare the results of the 105 mm HE projectile fragmentation given by the real experiment [14] and the numerical method. Fig.27 illustrates the distribution of the fragment number frequency depending on the fragment mass obtained for casing materials of relatively similar mechanical properties.

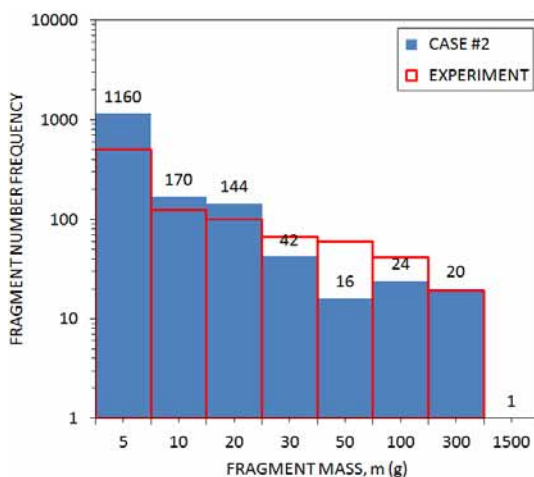


Figure 27. Fragment number frequency vs. fragment mass

The last histograms in Fig.27 indicate a good agreement of the experimental data and the numerical results (Case #2). Larger deviations occur in the fragment groups ranged about 5 g and 50 g.

The accomplished analyzes indicate an excellent performance of the solver used in the numerical simulation of projectile fragmentation. Its main disadvantage is the impossibility of introducing the effect of the chemical composition of casing materials (iron and shell-grade steels) in the analysis of the fragmentation process. One possible way to overcome it is by artificially adjusting one (or more) of the mechanical parameters of the casing material.

Conclusion

The numerical simulation of the fragmentation process varying the mechanical characteristics of the casing and type of filled explosive was successfully carried out. The used solver is able to determine a large variety of the parameters of fragmentation such as fragment velocity, fragment size and mass and fragment mass distribution. Furthermore, a few characteristics of casing fragmentation, immeasurable in real experiments, are computed and shown, e.g.: temperature, stress and strain and strain rates in the casing wall. Some results of the numerical simulation match well with the relevant experimental data.

Acknowledgement

Parts of this research were supported by the Ministry of Education and Science of the Republic of Serbia through the Mathematical Institute SANU Belgrade Grant OI174001 " -Dynamics of hybrid systems with complex structures. Mechanics of materials". The author would like to thank Dr Milan Bojanović, Director of CAD PROFESSIONAL SYS, for his support of the research and for facilitating the use of the licensed academic software ANSYS products.

References

- [1] DEHN, J.: *Probability formulas for describing fragment size distribution*, Ballistic research laboratory, Aberdeen Proving Ground, ARBRL-TR-02332, 1981.
- [2] GRADY, D.E.: *Investigation of explosively driven fragmentation of metals-two-dimensional fracture and fragmentation of metal shells*, Progress Report II, US. Department of Energy, Lawrence Livermore National Laboratory, UCRL-CR-152264, B522033, 2003.
- [3] ELEK, P., JARAMAZ, S.: *Fragment mass distribution of naturally fragmenting warheads*, FME Transactions, 2009, Faculty of Mechanical Engineering, Belgrade, Vol.37, pp.129-135.
- [4] VUKAŠINOVIĆ, M.: *Contribution to theory and practice of the experimental testing of fragmentation effect of the high explosive projectiles*, PhD dissertation, Military Technical Academy, Belgrade, 1999 (in Serbian)
- [5] JOVANOVIĆ, R.: *Evaluation of regularity of HE projectiles fragmentation using statistical tests*, MSc thesis, Faculty of Mechanical Engineering, University of Belgrade, Belgrade, 2002 (in Serbian)
- [6] ELEK, P., JARAMAZ, S.: *Modeling of fragmentation of rapidly expanding cylinders*, Theoret. Appl. Mech., Belgrade, 2005, Vol.32, No.2, pp.113-130.
- [7] Crull, M., Swisdak, M.: *Methodologies for calculating primary fragment characteristics*, Technical Paper, No.16, Department of Defense Explosives Safety Board Alexandria, VA, 2005.
- [8] ОРЛЕНКО, Л.П. (редактор): *Физика взрыва, издание третье, дополненное и переработанное*, под редакцией издательство «Наука», Главная редакция физико-математической литературы, Москва, 2004.
- [9] ĐURĐEVAC, D.: *Possibility of the FEM application for a stress condition analysis of an artillery projectile body*, Scientific Technical Review, ISSN 1820-0206, 2008, Vol.58, No.1, pp.3-8.
- [10] www.century-dynamics.com and www.ansys.com, Theory manual, Century Dynamics, Solutions through Software, Huston, USA.
- [11] BOLJANOVIĆ, S., MAKSIMOVIĆ, S., ĐURIĆ, M.: *Analysis of crack propagation using the strain energy density method*, Scientific Technical Review, ISSN 1820-0206, 2009, Vol.59, No.2, pp.12-17.
- [12] STAMATOVIĆ, A.: *Design of projectiles*, Ivexy, Belgrade, 1995.
- [13] TANAPORNRAWEEKIT, G., KULSIRIKASEM, W.: *Effects of material properties of warhead casing on natural fragmentation performance of high explosive (HE) warhead*, World Academy of Science, Engineering and Technology, 2011, Vol.59, pp.1275-1280.
- [14] UGRČIĆ, M.: *Fundamentals of projectile design and producing - Exercises with the theory abstracts*, VIZ, Military Academy Belgrade, 2008.

Numerička simulacija procesa fragmentacije razornih projektila

Najnovije proračunske tehnike, zasnovane na metodi konačnih elemenata (MKE), razvijene su u ciju rešavanja problema eksplicitne dinamike i mogu se primeniti u predikciji prirodne fragmentacije razornih projektila. Nova metodologija za numeričku simulaciju performansi fragmentacije projektila integriše MKE i teoriju stohastičkog loma u solveru ANSYS AUTODYN® za dvo- i trodimenzionalne osno-simetrične analize procesa fragmentacije. Rad prikazuje rezultate numeričkih analiza karakteristika fragmentacije iskazane kroz početnu brzinu, ugao razleta, raspodelu dužine i mase fragmenata za razorni projektil 105 mm. Karakteristike fragmentacije projektila zavise od oblika i veličine projektila, debljine košuljice, vrste eksploziva, veličine i položaja detonatora, itd. Težište rada je usmereno na uticaj mehaničkih karakteristika materijala košuljice i vrste eksploziva na parametre fragmentacije. Potvrđeno je da mehaničke karakteristike košuljice imaju mali uticaj na početnu brzinu parčadi. Pored toga, pokazano je da krti materijali košuljice sa malom kritičnom deformacijom produkuju veći broj fragmenata sa manjom vrednošću srednje mase fragmenata. U poređenju sa određenim eksperimentalnim podacima potvrđeno je da izračunati parametri fragmentacije korektno predviđaju karakteristike razaranja košuljice.

Ključne reči: razorni projektil, fragmentacija projektila, kalibar 105 mm, numerička simulacija, metoda konačnih elemenata.

Численное моделирование процесса фрагментации осколочных боевых частей

Последние расчётные методы, основанные на методе конечных элементов (МКЭ), разработаны для решения проблем в динамике в практике и могут применяться в прогнозировании природной фрагментации разрушительных снарядов. Новая методика численного моделирования характеристик фрагментации снаряда интегрирует МКЭ и теорию стохастического перелома решателя ANSYS автодинный® для двухмерного и трёхмерного осесимметричного анализа процесса фрагментации. В данной работе представлены результаты численного анализа характеристик фрагментации, которую сообщили через начальную скорость, угол фрагмента, распределение длины и массы фрагментов для разрушительного снаряда в 105 мм. Особенности фрагментации снаряда зависят от формы и размера снаряда, толщины рубашки, типа взрывчатых веществ, размера и положения детонаторов и так далее. Основное внимание в статье уделено влиянию механических свойств материалов рубашки и типа взрывчатого вещества на параметры фрагментации. Было подтверждено, что механические характеристики вкладыша-рубашки мало влияют на начальную скорость осколков. Кроме того, было показано, что хрупкие материалы рубашки с маленькой критической деформацией производят большее число фрагментов с более низким значением средней массы фрагментов. По сравнению с некоторыми определёнными экспериментальными данными было подтверждено, что параметры фрагментации были рассчитаны правильно и предсказывают характеристики разрушений рубашки.

Ключевые слова: разрушительные снаряды, фрагментация снаряда, калибр в 105 мм, численное моделирование, метод конечных элементов.

Simulation numérique du processus de la fragmentation des projectiles puissants

Les dernières techniques de computation basées sur la méthode des éléments finis (MEF) ont été développées dans le but de résoudre les problèmes de la dynamique explicite et elles peuvent s'appliquer pour la prédiction de la fragmentation des projectiles puissants. La nouvelle méthodologie de la simulation numérique des performances de la fragmentation des projectiles intègre la MEF et la théorie de la fracture stochastique dans le logiciel ANSYS AUTODYN pour les analyses axiales symétriques de fragmentation à deux et à trois dimensions. Ce travail présente les résultats des analyses numériques des caractéristiques de fragmentation exprimés par la vitesse initiale, l'angle de pulvérisation, la distribution de la longueur et de la masse des fragments pour le projectile puissant de 105mm. Les caractéristiques de la fragmentation du projectile dépendent de la forme et de la taille du projectile, de l'épaisseur de l'enveloppe, du type de l'explosif, de la taille et de la position de détonateur, etc. L'essentiel de ce travail est centré sur les effets que les caractéristiques mécaniques du matériel de l'enveloppe et du type de l'explosif font sur les paramètres de fragmentation. On a confirmé que les caractéristiques mécaniques de l'enveloppe avaient peu d'effet sur la vitesse initiale des fragments. En outre, on a démontré que les matériaux fragiles de l'enveloppe à petite déformation critique produisaient plus grand nombre de fragments à plus petite masse moyenne. La comparaison avec quelques données expérimentales a confirmé que les paramètres calculés de la fragmentation prévoiaient correctement les caractéristiques de la destruction de l'enveloppe.

Mots clés: projectile puissant, fragmentation de projectile, calibre 105mm, simulation numérique, méthode des éléments finis.